

DISCOVERY OF $Z \sim 8$ GALAXIES IN THE HUDF FROM ULTRA-DEEP WFC3/IR OBSERVATIONS¹

R. J. BOUWENS^{2,3}, G. D. ILLINGWORTH², P. A. OESCH⁴, M. STIAVELLI⁵, P. VAN DOKKUM⁶, M. TRENTI⁷, D. MAGEE², I. LABBÉ⁸, M. FRANX³, C. M. CAROLLO⁴, V. GONZALEZ²

Draft version October 29, 2018

ABSTRACT

We utilize the newly-acquired, ultra-deep WFC3/IR observations over the HUDF to search for star-forming galaxies at $z \sim 8 - 8.5$, only 600 million years from recombination, using a Y_{105} -dropout selection. The new 4.7 arcmin² WFC3/IR observations reach to ~ 28.8 AB mag (5σ) in the $Y_{105}J_{125}H_{160}$ bands. These remarkable data reach ~ 1.5 AB mag deeper than the previous data over the HUDF, and now are an excellent match to the HUDF optical ACS data. For our search criteria, we use a two-color Lyman-Break selection technique to identify $z \sim 8 - 8.5$ Y_{105} -dropouts. We find 5 likely $z \sim 8-8.5$ candidates. The sources have H_{160} -band magnitudes of ~ 28.3 AB mag and very blue UV -continuum slopes, with a median estimated β of $\lesssim -2.5$ (where $f_\lambda \propto \lambda^\beta$). This suggests that $z \sim 8$ galaxies are not only essentially dust free but also may have very young ages or low metallicities. The observed number of Y_{105} -dropout candidates is smaller than the 20 ± 6 sources expected assuming no evolution from $z \sim 6$, but is consistent with the 5 expected extrapolating the Bouwens et al. 2008 LF results to $z \sim 8$. These results provide evidence that the evolution in the LF seen from $z \sim 7$ to $z \sim 3$ continues to $z \sim 8$. The remarkable improvement in the sensitivity of WFC3/IR has enabled HST to cross a threshold, revealing star-forming galaxies at $z \sim 8-9$.

Subject headings: galaxies: evolution — galaxies: high-redshift

1. INTRODUCTION

An important uncharted frontier is understanding how galaxies build up and evolve from the earliest times. While great progress has been made in characterizing the galaxy population at $z \lesssim 6$, extending these studies to $z \gtrsim 7$ has proven extraordinarily challenging. Only ~ 25 high-quality $z \sim 7$ candidates are known (e.g., Bouwens et al. 2008; Oesch et al. 2009; Ouchi et al. 2009; Castellano et al. 2009; Gonzalez et al. 2009; R.J. Bouwens et al. 2009, in prep). Fundamentally, the challenge has been to obtain extremely deep observations in the near-IR, where the redshifted UV light of faint $z \gtrsim 7$ galaxies is found.

Now, with the installation of the WFC3/IR camera on HST, we have a far superior surveying instrument, with $6 \times$ the area of NICMOS, $\gtrsim 2 \times$ the resolution, and $2-4 \times$ the sensitivity. These capabilities allow us to search for $z \gtrsim 7$ galaxies $\sim 40 \times$ more efficiently.

Here we report on our use of the early WFC3/IR observations over the HUDF to search for galaxies at $z \gtrsim 8$. This is the same epoch in which a GRB was recently discovered at $z \sim 8.2$ (e.g., Salvaterra et al. 2009; Tanvir

et al. 2009). Throughout this work, we quote results in terms of the luminosity $L_{z=3}^*$ Steidel et al. (1999) derived at $z \sim 3$, i.e., $M_{1700,AB} = -21.07$. We refer to the F606W, F775W, F850LP, F105W, F125W, and F160W bands on HST as V_{606} , i_{775} , z_{850} , Y_{105} , J_{125} , and H_{160} , respectively, for simplicity. Where necessary, we assume $\Omega_0 = 0.3$, $\Omega_\Lambda = 0.7$, $H_0 = 70$ km/s/Mpc. All magnitudes are in the AB system (Oke & Gunn 1983).

2. HUDF WFC3/IR OBSERVATIONS

The present high redshift galaxy searches utilize the first epoch of ultra-deep near-IR WFC3/IR observations acquired over the HUDF (Beckwith et al. 2006) for the 192-orbit HUDF09 program (GO11563). This program will create three ultra-deep WFC3/IR fields, one positioned over the HUDF and the other two over the HUDF05 fields (Oesch et al. 2007), each imaged in three near-IR bands Y_{105} , J_{125} , and H_{160} . Combining these ultra-deep near-IR data with the similarly deep optical HUDF data permits us to select $z \sim 7$ z_{850} , $z \sim 8$ Y_{105} , and even $z \sim 10$ J dropout galaxies to very low luminosities (i.e., -18 AB mag, $\sim 0.06 L_{z=3}^*$).

The WFC3/IR field over the HUDF is centered on $3^h 32^m 38.5^s$ and $-27^d 47' 0.0''$. In the first year of observations, we obtained 16 orbits of Y_{105} -band data (2 orbits were severely impacted by persistence and are not included), 16 orbits of J_{125} -band data, and 28 orbits of H_{160} -band data. The 60-orbit observations were obtained from August 26, 2009 to September 6, 2009.

Standard techniques were used to reduce the HUDF09 WFC3/IR imaging data. Individual images – after masking out sources – were median stacked to create super median images (one per filter) and these median images were then subtracted from the individual frames. The images were then aligned and drizzled onto the same grid as the v1.0 HUDF ACS data (Beckwith et al. 2006) re-

¹ Based on observations made with the NASA/ESA Hubble Space Telescope, which is operated by the Association of Universities for Research in Astronomy, Inc., under NASA contract NAS 5-26555. These observations are associated with programs #11563, 9797.

² UCO/Lick Observatory, University of California, Santa Cruz, CA 95064

³ Leiden Observatory, Leiden University, NL-2300 RA Leiden, Netherlands

⁴ Institute for Astronomy, ETH Zurich, 8092 Zurich, Switzerland

⁵ Space Telescope Science Institute, Baltimore, MD 21218, United States

⁶ Department of Astronomy, Yale University, New Haven, CT 06520

⁷ University of Colorado, Center for Astrophysics and Space Astronomy, 389-UCB, Boulder, CO 80309, USA

⁸ Carnegie Observatories, Pasadena, CA 91101, Hubble Fellow

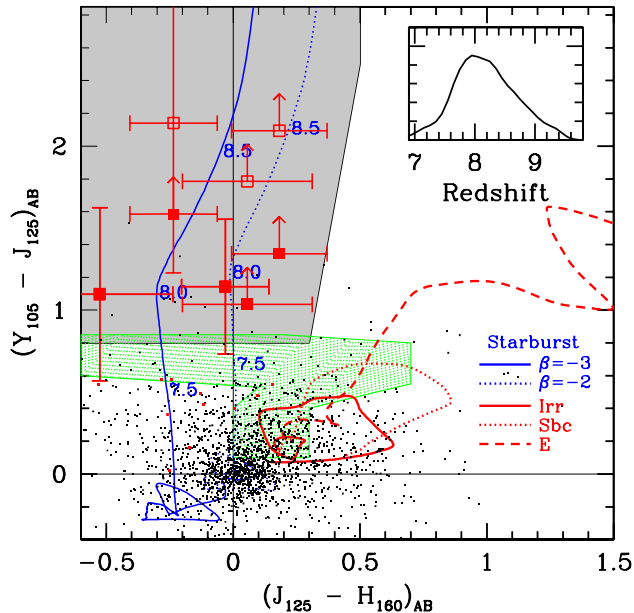


FIG. 1.— $Y_{105} - J_{125}$ vs. $J_{125} - H_{160}$ two-color selection used for identifying $z \sim 8$ Y_{105} -dropout galaxies in our HUDF WFC3/IR data. The colors of our 5 Y -dropout candidates are indicated with the large red squares (with 1σ error bars and 2σ limits: to be conservative) and open red squares (with 1σ limits). The blue lines show the colors expected for young star-forming galaxies (with UV continuum slopes $\beta = -3$ or $\beta = -2$) as a function of redshift. The solid, dashed, and dotted red lines show the colors we would expect for various low-redshift galaxy SEDs (Coleman et al. 1980). The hatched green region indicates the region in color space we would expect L,T dwarfs to lie (Knapp et al. 2004). The colors of individual sources in our photometric sample are given with the small black points (for those detected in the HUDF optical data and hence not included in our selection) and the small red points (for those undetected in the optical). The inset to the figure presents the expected redshift distribution for the sample using the simulations described in §4.1 and the fiducial LFs from §4.2. All of our $z \sim 8$ Y_{105} -dropout candidates have bluer UV -continuum slopes β than -2 (as indicated by their $J_{125} - H_{160}$ colors), with a median $\lesssim -2.5$. This suggests that $z \gtrsim 8$ galaxies are not only dust free but also probably have very young ages or low metallicities (see also Bouwens et al. 2010).

binned on a $0.06''$ -pixel scale. The drizzling was done using a modified version of multidrizzle (Koekemoer et al. 2002). 4σ outliers were rejected.

Given that the WFC3/IR instrument is still relatively new, we initially made our own estimates of the photometric zeropoints by performing PSF-matched photometry on sources present in both the new observations and the HUDF NICMOS observations (e.g., Thompson et al. 2005; Bouwens et al. 2008; Oesch et al. 2009). The zeropoints derived were consistent (<0.05 mag) with the official STScI values, so we elected to use the STScI values 26.27, 26.25, and 25.96 mag for the Y_{105} , J_{125} , and H_{160} bands, respectively. The approximate 5σ depths of the Y , J , and H WFC3/IR images are 28.8, 28.8, and 28.8 mag, respectively, in $0.4''$ -diameter apertures, ~ 1.5 mag deeper than the NICMOS data over the HUDF (Thompson et al. 2005). These depths were estimated by measuring the noise statistics in apertures of various size. The FWHM of the PSF in our WFC3/IR near-IR images is $\sim 0.16''$. For reference, the HUDF optical $B_{435}V_{606}i_{775}z_{850}$ data (Beckwith et al. 2006) reached to 29.4, 29.8, 29.7, and 29.0 AB mag (5σ : $0.35''$ -diameter

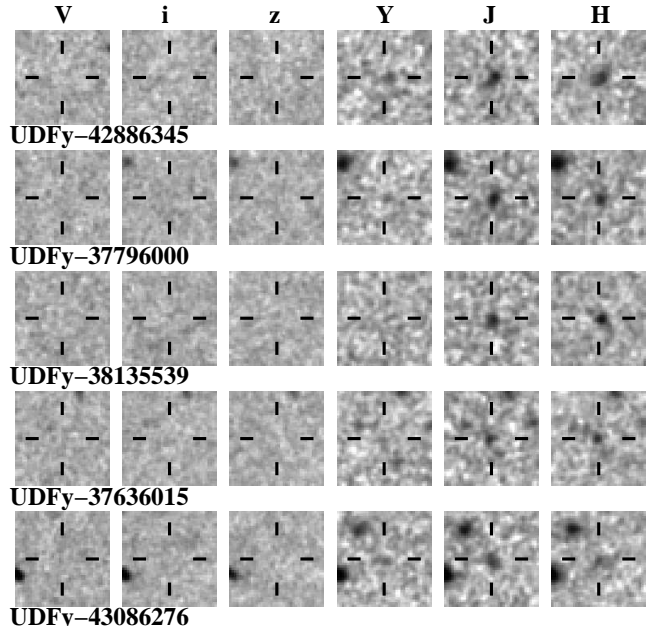


FIG. 2.— $V_{606}i_{775}z_{850}Y_{105}J_{125}H_{160}$ image cutouts ($2.4'' \times 2.4''$ on a side) of the five $z \sim 8$ Y_{105} -dropout candidates we identified in the ultra-deep HUDF WFC3/IR observations. All five candidates are detected at 5σ in both the J_{125} and H_{160} bands, but show no detection ($> 2\sigma$) in the ultra-deep optical HUDF V_{606} , i_{775} , or z_{850} band images.

apertures) and had PSF FWHMs of $\sim 0.10''$.

3. OBJECT DETECTION AND VERIFICATION

3.1. Catalog Construction

Our procedure for doing object detection and photometry is identical to that used in previous work (e.g., Bouwens et al. 2007; Bouwens et al. 2008) and is performed using SExtractor (Bertin & Arnouts 1996: run in dual-image mode) on the registered data. Object detection is done from the coadded J_{125} and H_{160} -band image (explicitly, using the square root of the χ^2 image: Szalay et al. 1999), both of which are redward of the break for Y_{105} -dropout galaxies. After smoothing the optical data to match the WFC3/IR PSFs, colors are measured using Kron (1980)-style photometry in small apertures that scale with the size of the source (for Kron factors of 1.2). Flux measurements in these small apertures are corrected up to total magnitudes using the flux in larger scalable apertures (Kron factors of 2.5). This correction to total magnitudes (see e.g. Figure 5 from Coe et al. 2006) is done on a source by source basis, based on the square root of χ^2 image (approximately proportional to the coadded flux). Finally, the total magnitudes were corrected by 0.1 mag to account for light on the wings of the PSF.

3.2. Dropout Selection

Sources are selected over 4.7 arcmin 2 with the deepest WFC3/IR observations ($\lesssim 10\%$ of this area is not at the full depth). The selection criteria we adopt for identifying $z \sim 8$ Y_{105} dropout galaxies are simple analogues of the criteria used to select Lyman Break galaxies at lower redshift (e.g., Steidel et al. 1996; Giavalisco et al. 2004; Bouwens et al. 2007). That is, we require galaxies to show strong breaks ($Y_{105} - J_{125} > 0.8$) at

TABLE 1
 $z \sim 8$ Y_{105} -DROPOUT CANDIDATES IDENTIFIED OVER OUR ULTRA-DEEP HU DF
 WFC3/IR FIELD.

Object ID	R.A.	Dec	H_{160}	$Y_{105} - J_{125}^a$	$J_{125} - H_{160}$
UDFy-42886345	03:32:42.88	-27:46:34.5	28.0 ± 0.1	1.1 ± 0.4	0.0 ± 0.2
UDFy-37796000	03:32:37.79	-27:46:00.0	28.0 ± 0.1	2.1 ± 0.9	-0.3 ± 0.2
UDFy-38135539	03:32:38.13	-27:45:53.9	28.1 ± 0.1	> 2.1	0.2 ± 0.2
UDFy-37636015	03:32:37.63	-27:46:01.5	28.4 ± 0.1	> 1.8	0.1 ± 0.3
UDFy-43086276	03:32:43.08	-27:46:27.6	29.0 ± 0.2	1.1 ± 0.5	-0.5 ± 0.3

^a Lower limits on the measured colors are the 1σ limits. Magnitudes are AB.

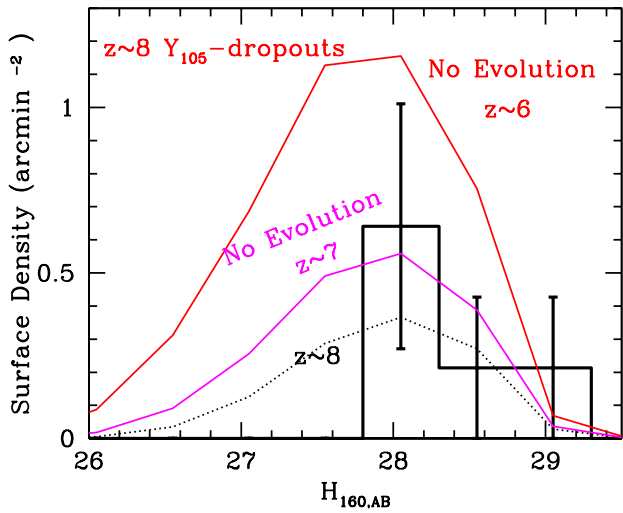


FIG. 3.— Surface density of $z \sim 8$ Y_{105} -dropouts found in our ultra-deep HUDF WFC3/IR field versus H_{160} -band magnitude. For comparison, the surface density of Y_{105} -dropouts one would expect assuming no evolution from $z \sim 6$ and $z \sim 7$ is also plotted (shown with the red and magenta lines, respectively: see §4.1). Also plotted (dotted black line) is the expected surface density if one extrapolates the $z \sim 4$ -6 LF results of Bouwens et al. (2008) to $z \sim 8$, i.e., with a ϕ^* of $\sim 0.0011 \text{ Mpc}^{-3}$, α of -1.74 , and a fainter value of M^* .

the redshifted position of Ly α at $z \sim 8$ and to be blue redward of the break, i.e., ($J_{125} - H_{160} < 0.5$) and ($J_{125} - H_{160}) < 0.2 + 0.12(Y_{105} - J_{125})$ to exclude intrinsically red galaxies at lower redshift (Figure 1). We also require our Y_{105} -dropout candidates to show no detection ($< 2\sigma$: color-measurement aperture) in all bands blueward of the dropout band, i.e., $B_{435}V_{606}i_{775}z_{850}$. Sources showing a $> 1.5\sigma$ detection in > 1 optical band were also eliminated. All of our Y_{105} -dropout candidates were required to be 5.5σ detections in the J_{125} band to ensure they corresponded to real sources. We elected to use a 5.5σ criterion to be conservative for these early WFC3/IR data.

The most stringent aspect of the current selection is our requirement that sources be undetected in the ultra-deep HUDF optical data (which reaches to 31.5-32.0 at 1σ for most sources). From our simulations (§3.4), this requirement eliminates almost all contamination from $z \lesssim 6$ galaxies, and hence we can use a modest ($Y_{105} - J_{125}) > 0.8$ break to select $z \sim 8$ galaxies, without significant contamination concerns.

3.3. Y_{105} -dropout Sample

We identify five sources that satisfy our Y -dropout criteria (see Table 1). The position of these sources in the

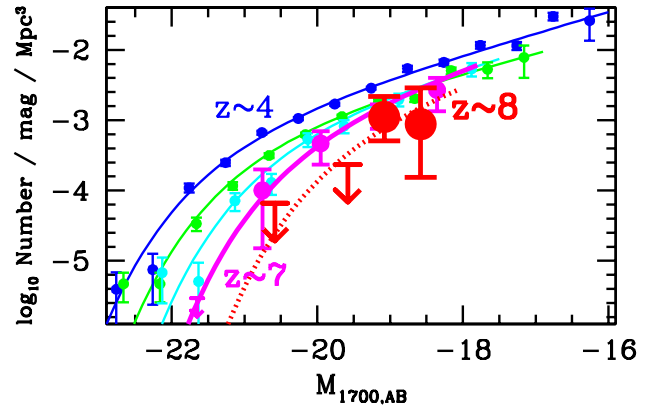


FIG. 4.— Constraints on the rest-frame UV LF at $z \sim 8$ from the present Y_{105} -dropout searches over our ultra-deep HUDF WFC3/IR field (solid red circles, 1σ error bars and upper limits). Also included is our UV LF determination at $z \sim 7$ from a z -dropout search over the same ultra-deep WFC3/IR field (magenta lines and points: Oesch et al. 2010a) and also the Bouwens et al. (2007) UV LF determinations at $z \sim 4, 5$ and 6 (shown in blue, green, and cyan lines and points). While the other UV LFs shown here were derived at slightly different rest-frame wavelengths, their $M_{UV,AB}$ at 1700\AA is essentially the same ($\lesssim 0.1 \text{ mag}$: since star-forming dropout galaxies are very flat in f_ν). The dotted red line gives one possible Schechter-like LF that agrees with our search results and adopts the Bouwens et al. (2008) scaling of M^* with redshift.

$Y_{105} - J_{125}/J_{125} - H_{160}$ two-color plane is given in Figure 1.⁹ The $J_{125} - H_{160}$ colors of our Y_{105} -dropout candidates are very blue in general, corresponding to UV-continuum slopes β of $\lesssim -2$ (where $f_\lambda \propto \lambda^\beta$), with a median $\beta \lesssim -2.5$ (though we emphasize the number of sources are still small and the inferred β 's may be affected by uncertainties in the photometry). The observed β 's are blue enough that $z \gtrsim 7$ galaxies must be essentially dust free, and possibly also have very young ages or metallicities (see also Bouwens et al. 2010).

Cutouts of the sources are provided in Figure 2. The candidates have $H_{160,AB}$ band magnitudes of ~ 28.0 - 29.0 AB mag, within one magnitude of our sensitivity limit. Such sources could not have been found to date since they are fainter than could be probed with other data sets. This illustrates the importance of the very deep near-IR data being collected as part of this program.

All five candidates have apparent half-light radii of $\sim 0.15''$ ($\sim 0.7 h^{-1} \text{ kpc}$) – measured using SExtractor – not much larger than the PSF. The 4 candidates – for which crowding is not a concern – do not show signifi-

⁹ It is encouraging that recently both McLure et al. (2010) and Bunker et al. (2010) have independently identified a very similar set of $z \sim 8$ candidates in the first epoch HUDF09 WFC3/IR observations over the HUDF.

cant ($>2\sigma$) detections in the IRAC data over the GOODS fields either individually or when stacked (Labbé et al. 2010). The non-detection of the candidates in the IRAC data is not particularly surprising given the much shallower depths of the IRAC data ($\lesssim 27.0$ AB mag at 2σ) relative to the WFC3/IR data.

3.4. Contamination Corrections

The only meaningful source of contamination for the present sample are sources that enter the selection via photometric scatter. A simple estimate of the likely contamination can be obtained by adding noise to the color distribution observed for ~ 25 - 26.5 AB mag galaxies. The advantage of using this color distribution for the simulations is that the distribution is realistic (being taken from the observations), has a higher S/N than at fainter magnitudes, and does not include any $z \gtrsim 7.5$ galaxies. We find $\lesssim 0.2$ contaminants per field, suggesting such a source of contamination is minimal ($\lesssim 4\%$).

The $< 4\%$ contamination estimate implicitly includes the contribution of $z \sim 1.5$ - 2 Balmer-Break Galaxies (BBG) sources scattered into our selection. We expect the explicit contribution to be small given the lack of faint sources with $V - J > 1.5$, $J - H > 0.15$ colors expected for BBGs (arbitrary reddenings, metallicities: R.J. Bouwens et al. 2010, in prep).

Other sources of contamination are not important for this selection. For example, given that each source is detected at $\geq 5.5\sigma$ in the J_{125} band and $\geq 4\sigma$ in the H_{160} band, no contamination from spurious sources is expected. Contamination by SNe is also not important, given that the $Y_{105}J_{125}H_{160}$ data were taken over the same 12-day window. Finally, contamination by stars is also unlikely. Not only are T dwarfs rare over the CDF-South, with a surface density $\lesssim 0.04$ arcmin $^{-2}$ (e.g., Bouwens et al. 2008) and therefore unlikely to be found in our 4.7 arcmin 2 field, but also all 5 of our candidates appear to be extended (having SExtractor stellarity parameters < 0.3 : see also Oesch et al. 2010b) and hence not likely to be stars.

4. RESULTS AND IMPLICATIONS

4.1. Expected Numbers

To interpret the results of the present $z \sim 8$ Y_{105} -dropout selection, it is useful to estimate how many Y_{105} -dropouts we might have expected if the UV LF showed no evolution from $z \sim 6$ and $z \sim 7$. We estimate the numbers by creating galaxy catalogs according to the model LFs, adding artificial galaxies to the data, and then processing the images and doing the selection in the same way as for the real data. For these simulations, we model the pixel-by-pixel profiles of galaxies at $z \sim 8$ with similar-luminosity galaxies from the $z \sim 4$ Bouwens et al. (2007) HUDF B dropout sample, but scaled in size to match the observed $(1+z)^{-1}$ size-redshift scaling (Oesch et al. 2010b; Bouwens et al. 2004, 2006; Ferguson et al. 2004). Star-forming galaxies at $z \sim 7-9$ are assumed to have mean UV-continuum slopes β of -2.5 , with a 1σ scatter of 0.4, to match the apparent colors of Y_{105} -dropouts in our sample (see Figure 1).

Adopting the $z \sim 6$ i -dropout LF from Bouwens et al. (2007: see also McLure et al. 2009) and assuming no evolution to higher redshift, we predict 20 ± 6 Y_{105} -dropouts

TABLE 2
UV LUMINOSITY DENSITIES AND STAR FORMATION RATE DENSITIES.^a

Dropout Sample	$\langle z \rangle$	$\log_{10} \mathcal{L}$	\log_{10} SFR density	
		($\text{ergs s}^{-1} \text{ Mpc}^{-3}$)	($M_{\text{odot}} \text{ Mpc}^{-3} \text{ yr}^{-1}$)	Uncorrected
z	6.8	25.73 ± 0.16^c	-2.17 ± 0.16	-2.17 ± 0.16
Y	8.2	25.18 ± 0.24	-2.72 ± 0.24	-2.72 ± 0.24

^a Integrated down to -18.3 AB mag, or $0.08 L_{z=3}^*$.

^b The dust correction is taken to be 0, given the very blue β 's (see also Bouwens et al. 2009; Bouwens et al. 2010)

^c Using the $z \sim 7$ UV LF derived from the same ultra-deep WFC3/IR field as this study (Oesch et al. 2010a)

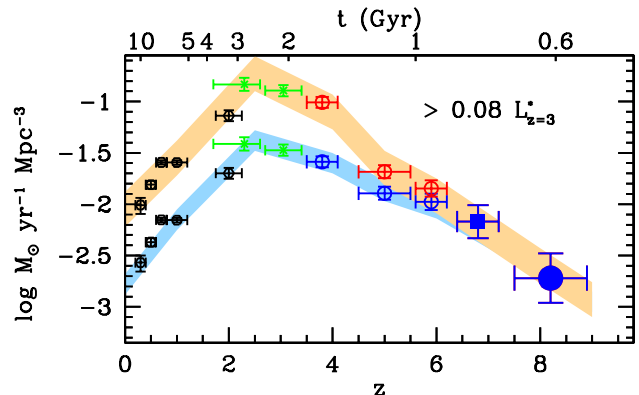


FIG. 5.— Determinations of the UV luminosity density and SFR density, integrated to $0.08 L_{z=3}^*$ (-18.3 AB mag) as appropriate for the $z \sim 8$ sample, as a function of redshift. The large red circle shows the constraints we can set on this density at $z \sim 8$ from the current Y_{105} -dropout search (see also §4.3). The lower set of points (and blue region) show the SFR density determination inferred directly from the UV light, and the upper set of points (and orange region) show what one would infer using dust corrections inferred from the UV-continuum slope measurements (e.g., Bouwens et al. 2009; Bouwens et al. 2010). Note that the dust correction is essentially zero at $z > 6$. Also included on this figure are the determinations at $z \sim 7$ from the HUDF WFC3/IR z -dropout search (Oesch et al. 2010a: *solid red square*), the Bouwens et al. (2007) determination at $z \sim 4-6$ (*open red circles*), the Reddy & Steidel (2009) determinations at $z \sim 2-3$ (*green crosses*), and the Schiminovich et al. (2005) determinations at $z \lesssim 2$ (*black hexagons*). A systematic increase in the SFR density from $z \sim 8$ to $z \sim 2$ is clear.

in our WFC3/IR field. The $z \sim 6$ predictions are shown as a function of H_{160} -band magnitude in Figure 3 and compared with the observations. We expect $\sim 70\%$ uncertainties in these numbers due to small number statistics and large-scale structure variations (assuming a 4.7 arcmin 2 survey field, $\Delta z \sim 0.8$ redshift selection window, and $\sim 10^{-3}$ Mpc $^{-3}$ source density: e.g., Trenti & Stiavelli 2008). The observed numbers are $> 2\sigma$ lower than expected from the well-determined $z \sim 6$ LF. Predicted surface densities can also be made using the Bouwens et al. (2008) $z \sim 7$ LF (also shown), but the uncertainties are large given the small sample in that paper (and the new WFC3/IR observations permit much better $z \sim 7$ LF estimates).

4.2. Implications for the $z \sim 8$ UV LF

The fact that the observed numbers are lower than predicted assuming no-evolution from $z \sim 6$ suggests that the UV LF continues to evolve from $z \sim 8$. So, it is in-

interesting to extrapolate the LF results from Bouwens et al. (2008) to $z \sim 8$ – giving $M_{UV}^* = -19.45$, $\phi^* \sim 0.0011$ Mpc^{-3} , and $\alpha \sim -1.74$ – and see what we find. Performing this exercise, we predict that 5 Y_{105} -dropouts would be found in the present search (*shown with the dotted black line in the lower panel of Figure 4*). This is in good agreement with the observed results.

We can further quantify the overall magnitude of this evolution. Using the Bouwens et al. (2008) LF parameterization as a guide, we fix $\alpha = -1.74$, $\phi^* = 0.0011$ Mpc^{-3} , and then derive confidence intervals on M_{UV}^* . For our Y_{105} -dropout search, we estimate that $M_{UV}^* = -19.5 \pm 0.3$ AB mag. This is significantly fainter than the $M_{UV}^* = -20.2 \pm 0.2$ AB mag estimated at $z \sim 6$ or the $M_{UV}^* = -21$ AB mag at $z \sim 4$.

Of course, given the size of the sample and lack of complementary wide-area searches for bright $z \sim 8$ sources, it is difficult to constrain the shape of the $z \sim 8$ UV LF. Therefore, we simply consider the stepwise LF at $z \sim 8$. We divide our dropout sample into 0.5 mag bins, compute the equivalent absolute magnitudes in each of these bins, and then divide the observed number of sources in each bin by the effective selection volume, which are estimated using the same simulations described in §4.1. These stepwise LF determinations are presented in Figure 4, with the LFs at $z \sim 4-7$ (Bouwens et al. 2007; Oesch et al. 2010a) shown for context. The 1σ upper limits on the volume density of luminous $z \sim 8$ sources are also shown. It would appear that the UV LF only shows very weak evolution at low luminosities (~ -18.3 AB mag). This is in contrast to the dramatic evolution observed at the bright end from $z \sim 7$ to $z \sim 4$ (see e.g. discussion in Shimasaku et al. 2005; Bouwens et al. 2008).

4.3. Constraints on the UV Luminosity Density/SFR density at $z \sim 8$

Finally, we calculate the luminosity densities (and unobscured SFR densities) at $z \sim 8$ implied by these constraints on the rest-frame UV LF. For the luminosity density at $z \sim 8$, we simply integrate the stepwise $z \sim 8$ LF shown in Figure 4. We convert these UV luminosity densities into the equivalent unobscured SFR densities using the Madau et al. (1998) prescription. The results are presented in Figure 5 and Table 2. Also presented are the star formation rate densities inferred. The dust correction is taken to be 0, given the very blue β 's (see also Bouwens et al. 2009; Bouwens et al. 2010).

As these results demonstrate, the remarkable improvement in the sensitivity and the “discovery efficiency” (area gain \times sensitivity gain) of WFC3/IR has enabled HST to cross a threshold. HST can now find star-forming galaxies at $z \sim 8-8.5$. The existence of such galaxies and the active star formation implied at even higher redshifts $z > 10$ provides a striking framework for future detailed JWST observations.

We acknowledge our program coordinator William Januswieski for his exceptional care in helping to set up our program and observing configuration. We are grateful to all those at NASA, STScI and throughout the community who have worked so diligently to make Hubble the remarkable observatory that it is today. The servicing missions, like the recent SM4, have rejuvenated HST and made it an extraordinarily productive scientific facility time and time again. We greatly appreciate the support of policymakers, and all those in the flight and servicing programs who contributed to the repeated successes of the HST servicing missions. We acknowledge the support of NASA grant NAG5-7697 and NASA grant HST-GO-11563.01. PO acknowledges support from the Swiss National Foundation.

REFERENCES

- Beckwith, S. V. W., et al. 2006, *AJ*, 132, 1729
 Bertin, E. and Arnouts, S. 1996, *A&AS*, 117, 39
 Bouwens, R. J., Illingworth, G. D., Blakeslee, J. P., Broadhurst, T. J., & Franx, M. 2004, *ApJ*, 611, L1
 Bouwens, R.J., Illingworth, G.D., Blakeslee, J.P., & Franx, M. 2006, *ApJ*, 653, 53
 Bouwens, R. J., Illingworth, G. D., Franx, M., & Ford, H. 2007, *ApJ*, 670, 928
 Bouwens, R. J., Illingworth, G. D., Franx, M., & Ford, H. 2008, *ApJ*, 686, 230
 Bouwens, R. J., et al. 2009, *ApJ*, 705, 936
 Bouwens, R. J., et al. 2010, *ApJ*, 708, L69
 Bunker, A., et al. 2010, *MNRAS*, in press, arXiv:0909.2255
 Castellano, M., et al. 2010, *A&A*, in press, arXiv:0909.2853
 Coe, D., Benítez, N., Sánchez, S. F., Jee, M., Bouwens, R., & Ford, H. 2006, *AJ*, 132, 926
 Coleman, G. D., Wu, C.-C., & Weedman, D. W. 1980, *ApJS*, 43, 393
 Ferguson, H. C. et al. 2004, *ApJ*, 600, L107
 Giavalisco, M., et al. 2004, *ApJ*, 600, L103
 Gonzalez, V., Labbé, I., Bouwens, R., Illingworth, G., Franx, M., Kriek, M., Brammer, G. 2009, *ApJ*, submitted, arXiv:0909.3517
 Koekemoer, A. M., Fruchter, A. S., Hook, R. N., & Hack, W. 2002, The 2002 HST Calibration Workshop : Hubble after the Installation of the ACS and the NICMOS Cooling System, 337
 Knapp, G. R., et al. 2004, *AJ*, 127, 3553
 Kron, R. G. 1980, *ApJS*, 43, 305
 Labbé, I., et al. 2010, *ApJ*, 708, L26
 Madau, P., Pozzetti, L., & Dickinson, M. 1998, *ApJ*, 498, 106
 McLure, R. J., Cirasuolo, M., Dunlop, J. S., Foucaud, S., & Almaini, O. 2009, *MNRAS*, 395, 2196
 McLure, R., et al. 2010, *MNRAS*, in press, arXiv:0909.2437
 Oesch, P. A., et al. 2007, *ApJ*, 671, 1212
 Oesch, P. A., et al. 2009, *ApJ*, 690, 1350
 Oesch, P. A., et al. 2010a, *ApJ*, 709, L16
 Oesch, P. A., et al. 2010b, *ApJ*, 709, L21
 Oke, J. B., & Gunn, J. E. 1983, *ApJ*, 266, 713
 Ouchi, M., et al. 2009, *ApJ*, 706, 1136
 Reddy, N. A., & Steidel, C. C. 2009, *ApJ*, 692, 778
 Salvaterra, R., et al. 2009, *Nature*, 461, 1258
 Schiminovich, D., et al. 2005, *ApJ*, 619, L47
 Shimasaku, K., Ouchi, M., Furusawa, H., Yoshida, M., Kashikawa, N., & Okamura, S. 2005, *PASJ*, 57, 447
 Steidel, C. C., Giavalisco, M., Pettini, M., Dickinson, M., & Adelberger, K. L. 1996, *ApJ*, 462, L17
 Steidel, C. C., Adelberger, K. L., Giavalisco, M., Dickinson, M., and Pettini, M. 1999, *ApJ*, 519, 1
 Szalay, A. S., Connolly, A. J., & Szokoly, G. P. 1999, *AJ*, 117, 68
 Tanvir, N. R., et al. 2009, *Nature*, 461, 1254
 Thompson, R. I., et al. 2005, *AJ*, 130, 1
 Trenti, M., & Stiavelli, M. 2008, *ApJ*, 676, 767